https://doi.org/10.22226/2410-3535-2022-4-388-393

Check for updates

Effect of homogenization on the structure, hardness and corrosion resistance of 1570C alloy

E. V. Avtokratova†, O. Sh. Sitdikov, R. R. Zagitov, M. V. Markushev

†avtokratova@imsp.ru

Institute for Metals Superplasticity Problems, RAS, Ufa, 450001, Russia

Influence of homogenizing annealing on the parameters of grain structure, phase constituents involving nanoscale aluminides of transition metals, hardness and corrosion resistance of the aluminum alloy 1570C (Al-5Mg-0.18Mn-0.2Sc-0.08Zr, mass.%) ingot was studied to optimize its heat treatment regimes according to a two-stage annealing scheme. At the first step, the ingot was annealed at 360°C for 6 hours (conventional route). At the second step, the annealing was performed at various temperatures in the range of 400 – 520°C for 1 hour. It was found, that additional high-temperature annealing resulted in some reduction in the alloy strength. However, it was quite effective to eliminate the chemical heterogeneity of the cast structure and increase the corrosion resistance maintaining grain size, dispersity and coherency of $Al_3(Sc, Zr)$ precipitates.

Keywords: aluminum alloy, homogenization, nanoscale dispersoids, hardness, corrosion.

1. Introduction

The aim of the present study was to optimize the heat treatment regimes of ingots out of the 1570C alloy through multistep homogenization. The alloy is one of the most high-strength ones among age-unhardenable aluminum alloys owing to its relatively high magnesium content and the presence of transition metals as Sc and Zr which provide solid solution and dispersion strengthening, respectively [1, 2]. The latter is mainly realized via precipitation of the $Al_3(Sc, Zr)$ phases coherent with the matrix, due to the decomposition of the supersaturated solid solution during homogenization of the ingot. These precipitates are commonly of nanoscale size and provide, along with the dispersion hardening, structure stabilization and structural strengthening [3 – 8]. However, the size and density of the precipitates depend on the regimes of heat treatment. Namely, the lower the temperature and duration of annealing, the more dispersed phases are formed causing a higher alloy strengthening [9 –12]. However, low-temperature homogenization is usually not enough to eliminate chemical heterogeneity arising during crystallization. Therefore, the issue of optimal modes and regimes of heat treatment of ingots out of 1570-type alloys still remains open at present. One of the approaches is to perform multistage homogenization with implementation of additional high-temperature annealing step.

2. Materials and experimental methods

The ingot of commercial alloy 1570C with the chemical composition Al-5Mg-0.18Mn-0.20Sc-0.08Zr (in mass.%) was subjected to multistep homogenization according to the scheme of two-stage annealing. First, the ingots were annealed at 360°C for 6 hours (conventional regime recommended by the developers of the alloy [13]). At the second step, the annealing was carried out at various temperatures in the range of 400 – 520°C for 1 hour.

The data on the alloy microstructure and the distribution of misorientations of (sub)boundaries were derived from scanning electron microscopy (SEM) with electron backscattering diffraction (EBSD) analysis using a TESCAN MIRA 3 LMH scanning electron microscope equipped with a field emission gun and HKL Channel 5 software. On the EBSD maps obtained, low-angle boundaries (LABs) corresponding to misorientation angles between adjacent scan points of $2° \le \Theta < 15°$, and high-angle boundaries (HABs) with misorientations of $\Theta \ge 15°$ were marked with white and black lines, respectively. Boundaries with misorientation angles less than 2° were not accounted among the analyzed boundaries. The alloy chemical and phase compositions were characterized on a TESCAN VEGA3 LMH scanning electron microscope equipped with an energy dispersive X-ray spectrometer (EDS). Precipitates were analyzed by transmission electron microscopy (TEM) using a JEOL-2000EX microscope equipped with an Oxford EDS system.

The objects for TEM and SEM analyses were prepared by electropolishing on a Tenurol-5 device in a solution of 30% HNO_3 and 70% CH_3OH at 20 V and at $T = -28$°C. The (sub)grain sizes were quantified by SEM-EBSD analysis through "equivalent diameter" as recommended in [14]. The size and distribution of $Al_3(Sc, Zr)$ precipitates were estimated from dark-field TEM images [15]. The phase number density was determined as the ratio of the number of precipitates to the TEM-image area and the foil thickness. The latter was determined by the number of extinction contours on the grain boundaries [15]. The Vickers microhardness (HV) was measured at room temperature on a semi-automatic "Metrotest" unit at a load of 0.5 N.

The corrosion resistance was examined by gravimetric analysis [16]. Before the test, the samples were brought to

a constant weight, cleaned, washed with alcohol and then weighed on analytical scales. The samples were then placed in the corrosive medium (1M HCl) at 25°C for 55 hours. After the test, the samples were washed in water, treated with alcohol, dried and weighed on analytical scales to measure the weight loss Δm. The weight loss during the exposition time was converted into the value of corrosion rate K_m, as follows [16]: $K_m = \Delta m / S \times t$, where Δm is the weight loss (g), S is the exposure area (m^2), and t is the exposure time (hours). Visible traces of corrosion both on the surfaces of the samples and in the center of their cross-sections after cutting and polishing were analyzed using the TESCAN MIRA 3 LMH scanning electron microscope. To ensure reliable results, at least 3 samples were evaluated in each state.

3. Results and discussions

The microhardness of the ingot after the first step of homogenization (360°C, 6 h) was 106 HV (Fig. 1). The subsequent one-hour annealing in the temperature range of 400 – 450°C did not contribute significantly to the changes in the alloy hardness. Noticeable softening of the alloy was observed after annealing at temperatures above 450°C with hardness decrease to 89 HV at 520°C.

Microstructure analysis has shown an absence of a noticeable effect of the second step of the ingot homogenization in the investigated temperature range on both the grain size and the angular characteristics of boundaries. Thus, after the first step of homogenization, the average grain size (d) was about 25 μm with the fraction of high-angle boundaries (f_{HABs}) and the average misorientation angle of the intercrystalline boundaries (Θ_{ave}) about 0.90 and 40.1°, respectively (Fig. 2 a, b). Meanwhile, the second homogenization step performed at the maximum temperature of 520°C (Fig. 2 c, d) resulted in only a slight increase in the grain size (to 27 μm) and the angular characteristics (to 0.92 (f_{HABs}) and 41.4° (Θ_{ave})).

At the same time, it was found that rather coarse metastable phases Al_3Mg_2/Al_8Mg_5 were located at the grain boundaries mainly after the first homogenization step (Fig. 3 a – e). These phases were inherited from the cast structure and indicated incomplete homogenization, even though the annealing temperature of 360°C was significantly higher than the solvus point for Mg in this alloy (250°C). Conducting even a much shorter second step but at higher temperatures resulted in more homogeneous distribution of the major alloying elements over the material volume and complete dissolution of the metastable phases by 520°C (Fig. 3 e – f). In spite of the solid-solution hardening, due to the increased Mg content

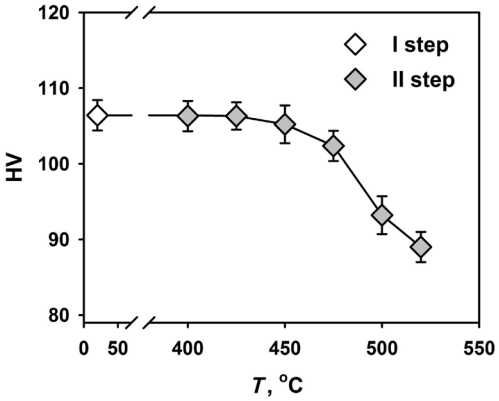

Fig. 1. Effect of temperature of 1-hour second step homogenization on the microhardness of the 1570C alloy ingot annealed in the first step at T = 360°C for 6 hours.

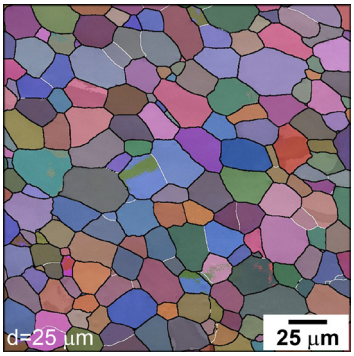

a

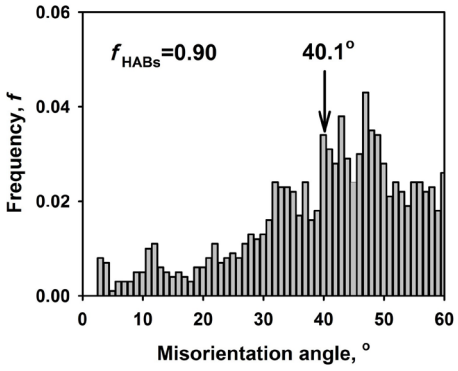

b

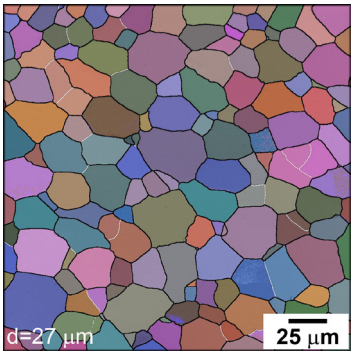

c

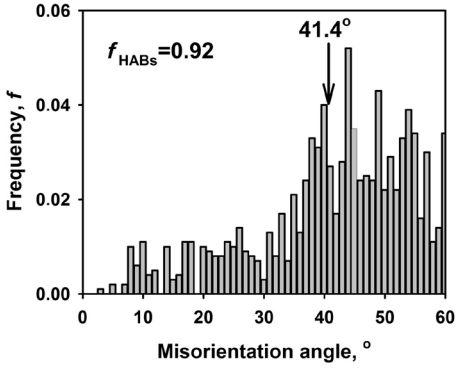

d

Fig. 2. (Color online) EBSD maps (a, c) and misorientation spectra of intergranular boundaries (b, d) of the alloy 1570C after the first (at 360°C, 6 h) (a, b) and second (at 520°C, 1 h) (c, d) homogenization steps.

in the aluminum matrix through additional dissolution of excess phases, the hardness of the alloy after the two-step homogenization was still noticeably lower than after the one-step homogenization. Considering that the average grain size practically did not change during the annealing, such behavior of the alloy could be caused only by changes in the parameters of aluminides of transition metals developed during both homogenization steps [3].

TEM analysis showed that after the first homogenization step, $Al_3(Sc, Zr)$ precipitates of about 5–10 nm in diameter with a number density of about 2×10^4 μm^{-3} were distributed relatively uniformly in the grain interiors (Fig. 4 a – c). The appearance of delta-zero contrast at these dispersoids in bright-field images (Fig. 4 a), as well as the presence of fine phase reflexes at around 1/2-typed positions being halfway between matrix strong reflections in the selected area

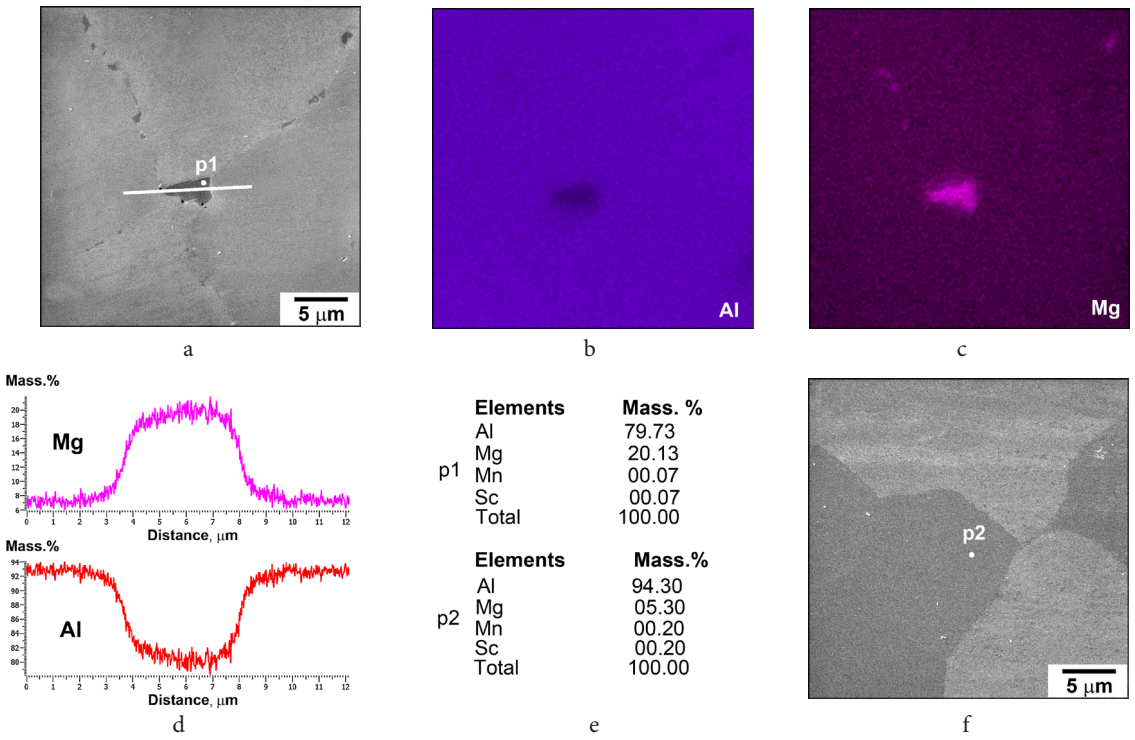

Fig. 3. (Color online) Microstructure of the alloy 1570C after the first homogenization step at $T = 360$°C for 6 h (a – d) and the second step at $T = 520$°C for 1 h (f). (a, f) — scanning electron microscopy; (b, c, d, e) — energy dispersion analysis of the structure in (a) and (f): (b, c) by area — maps of the distribution of elements in (a); (d) along the reference line in (a); (e) in the points p1 in (a) and p2 in (f).

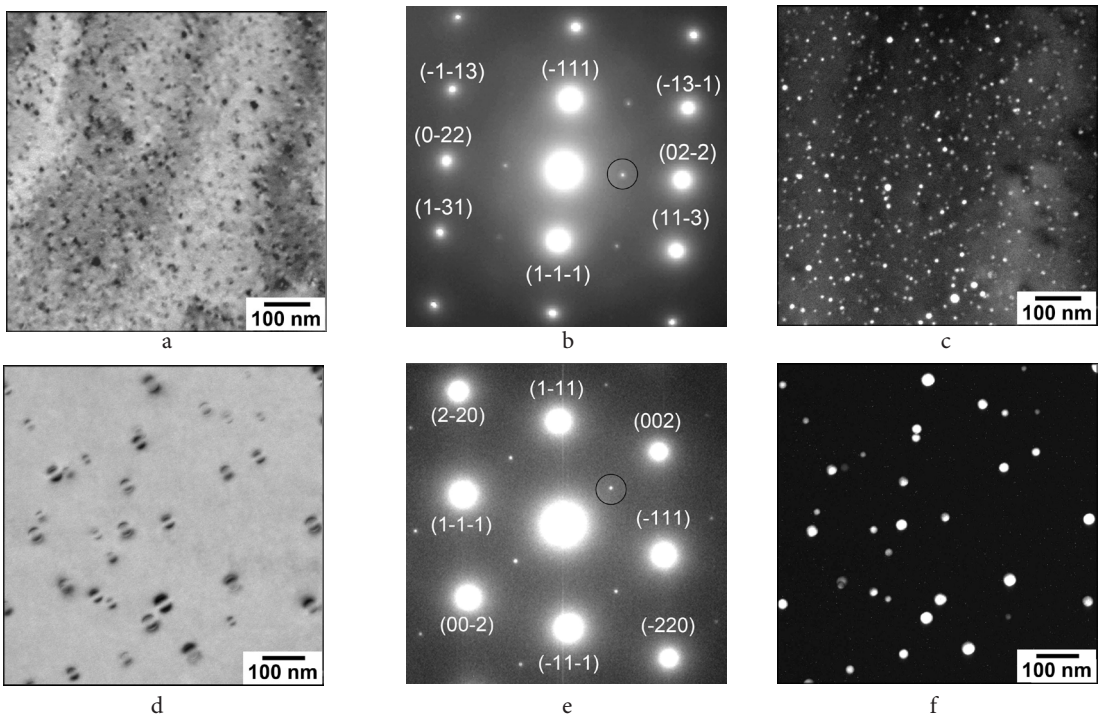

Fig. 4. TEM images of the alloy 1570C after the first homogenization step at $T = 360$°C for 6 h (a – c) and the second one at $T = 520$°C for 1 h (d – f); bright fields (a, d), SAEDs (b, e), and corresponded dark fields (c, f); black circles in SAEDs indicate the diffraction spots, from which the dark field patterns were obtained; (b) [211] zone axis and (e) [110] zone axis.

electron diffraction (SAED) patterns (Fig. 4 b), indicates that the precipitates were coherent with the matrix [3,15]. As expected, the subsequent high-temperature annealing resulted in the coarsening of the precipitates and a decrease in their density. Thus, after annealing at 520°C, the size of the dispersoids increased to 20 – 50 nm with an appropriate decrease in their density to 5×10^3 μm^3 (Fig. 4 d – f). At the same time, dispersoids despite their coarsening predominantly maintained their coherency with the matrix. This is confirmed by the retention of their delta-zero contrast in bright-field TEM images (Fig. 4 d), as well as by characteristic phase reflexes in SAED patterns with corresponding dark-field TEM images (Fig. 4 e, f). It should be noted that these results are in good agreement with the data of [17,18], which pointed out that $Al_3(Sc, Zr)$ dispersoids up to 100 nm in diameter retain their coherency in Al-Mg-Sc-Zr alloys.

Another structural feature of the homogenized alloy was the presence of grain boundary precipitate-free zones (PFZs) with only chains of much coarser Sc-rich precipitates (Fig. 5). The formation of such zones is typical for age-

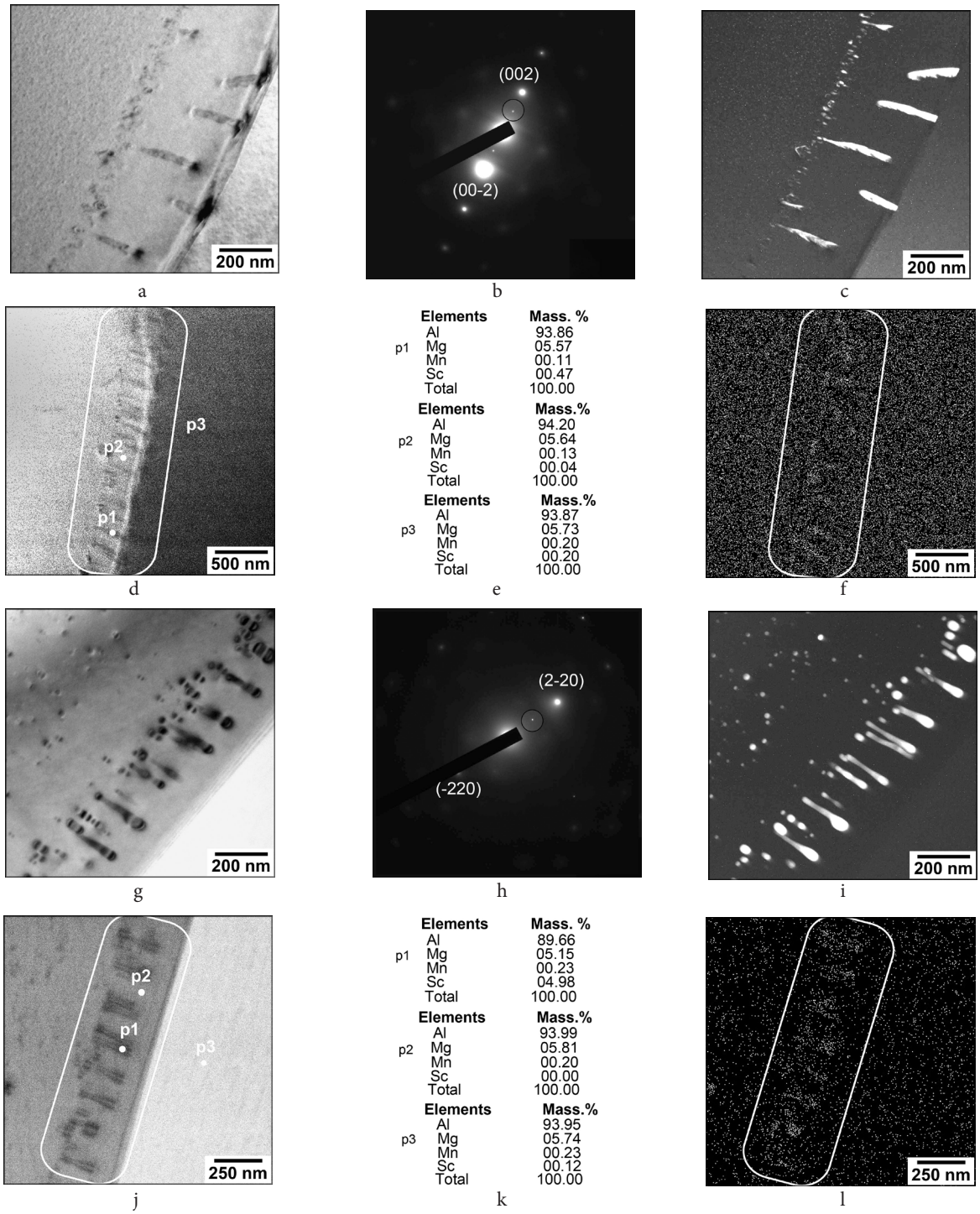

Fig. 5. Microstructures of the alloy 1570C after the first homogenization step at $T = 360$°C for 6h (a – f) and the second one at $T = 520$°C for 1 h (g – l); (a – c, g – i) TEM: bright fields (a, g), SAEDs (b, h), and corresponded dark fields (c, i); black circles in SAEDs indicate the diffraction spots, from which the dark field patterns were obtained; (b) [100] zone axis and (h) [110] zone axis; (d-f, j-l) EDS analysis: in the points p1-p3 (d, e and j, k) and corresponding maps of Sc distribution (f, l).

hardenable aluminum alloys, in which the decomposition of the aluminum solid solution and dispersion hardening are necessary attributes of their property control [19]. During homogenization of the present age-unhardenable alloy, the decomposition of the abnormally supersaturated solution of transition metals in aluminum took place, which had the same origin, proceeded by the same mechanisms and led to formation of similar structural components. As the result, besides the formation of PFZs, some intense coarsening of aluminides occurred in the grain boundary regions. The most common reasons for that can be the higher diffusion rate of dissolved atoms of Sc (Zr) along the high-angle boundaries, if compared to that in the grain interiors [20]. It may also be suggested that the clusters/chains of coarser phases as well as fan-shaped zones of coarse particle aggregations represented in Fig. 5 are also the result of activity of another precipitation mechanism (i.e., discontinuous precipitation) operated in the grain boundary region during homogenization, as described elsewhere [21]. The observation of alternating Sc-rich (points p1) and Sc-depleted (points p2) areas in the fan-shaped aggregation zones compared to the adjacent matrix (points p3) (Fig. 5 d – f and j – l) supports this assumption. It is also necessary to note that after the second high-temperature stage, the scandium content in the enriched areas (p1) was several times higher compared to the state homogenized at 360°C only.

The results of the assessment of corrosion damage of the alloy subjected to the one- and two-step homogenization, upon its immersion in HCl, are shown in Fig. 6. It is known that hydrochloric acid is highly aggressive even to easily passivating aluminum due to its content of chloride ions, which contribute to the formation of pitting [22]. However, it can be seen in Fig. 6 a, b that the samples, homogenized at the low temperature, were more severely corroded. Therewith, the corrosion rate in the samples after the first step was almost 4 times higher than after the second one (K_m=15.2 ± 2.0 and 4.1± 0.6 g/m^2×h, respectively). It was also evident after specimen preparation (Fig. 6 c, d) that significant material damage occurred after the first step along the grain boundaries due to intense occurrence of intergranular corrosion. Thus, corrosion processes were most active in the sample homogenized according to the one-step route. This result is due to the fact that the alloy contains a less equilibrium solid solution and, as follows from Fig. 3, a respectable amount of metastable phases along the grain boundaries. Consequently, it is characterized by pronounced chemical and structural heterogeneity, which contributes to the strengthening of corrosion. Corrosion damage increases with the number of nonequilibrium phases playing the role of corrosion centers [22]. In this regard, even a small number of centers can lead to a sharp increase in the rate of corrosion in the alloy. On the contrary, the formation of a more equilibrium structure after the second step of homogenization, namely, additional dissolution of excess phases and balancing the composition of solid solution in terms of magnesium content slowed the corrosion.

4. Conclusions

The effect of homogenizing annealing carried out at 360°C for 6 hours (first step) and then at up to 520°C for 1 hour (second step) on the structure, hardness and corrosion resistance

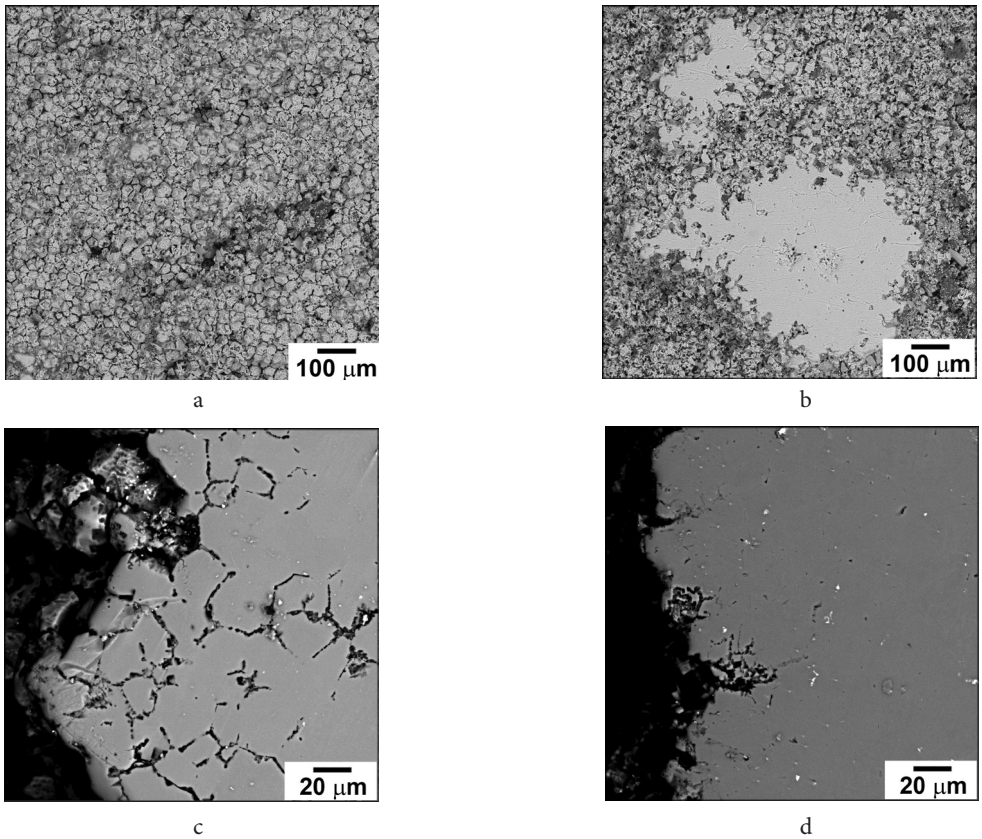

a b c d

Fig. 6. SEM images showing the corrosion damage of the samples out of the alloy 1570C after the first homogenization step at T = 360°C for 6 h (a, c) and the second one at T = 520°C for 1 h (b, d); (c, d) show lateral polished surfaces.

of aluminum alloy 1570C (Al-5Mg-0.18Mn-0.2Sc-0.08Zr, mass.%) ingot was studied. It was shown that the single-step (low-temperature) homogenization, recommended by the alloy developers, did not lead to the complete removal of chemical heterogeneity arising during crystallization. An additional high-temperature annealing step resulted in some reduction in the alloy strength, but was effective in eliminating the chemical heterogeneity of the cast structure and increasing corrosion resistance while maintaining the grain size and dispersity and coherency of the nanosized $Al_3(Sc, Zr)$ precipitates present in the alloy.

Acknowledgements. The work was supported by the Ministry of Science and Higher Education of Russian Federation through the state assignment of IMSP RAS (AAAA-A19-119021390107-8). It was performed using the facilities of the shared services center "Structural and Physics-Mechanical Studies of Materials" at the Institute for Metals Superplasticity Problems of Russian Academy of Sciences.

References

1. Yu. A. Filatov, V. I. Yelagin, V. V. Zakharov. Mater. Sci. Eng. A. 280 (1), 97 (2000). Crossref
2. V. V. Zakharov. Metal Science and Heat Treatment. 45 (7 – 8), 246 (2003). Crossref
3. O. N. Senkov, M. R. Shagiev, S. V. Senkova, D. B. Miracle. Acta Mater. 56, 3723 (2008). Crossref
4. L. Liu, J.-T. Jiang, B. Zhang, W.-Z. Shao, L. Zhen. J. Mater. Sci. Technol. 35 (6), 962 (2019). Crossref
5. B. Rouxel, M. Ramajayam, T. J. Langan, J. Lamb, P. G. Sanderse, T. Dorin. Materialia. 9, 100610 (2020). Crossref
6. O. Sitdikov, E. Avtokratova, M. Markushev. Metal. Mater. Int. 27, 2743 (2021). Crossref
7. E. Avtokratova, O. Sitdikov, M. Markushev, M. Linderov, D. Merson, A. Vinogradov. Mater. Sci. Eng. A. 806, 140818 (2021). Crossref
8. L. Jiang, B. Rouxel, T. Langan, T. Dorin. Acta Mater. 206, 116634 (2021). Crossref
9. A. A. Ragazin, V. V. Yashin, I. A. Latushkin, E. V. Aryshesnkii, F. V. Grechnikov. Mater. Sci. Forum. 1049, 102 (2022). Crossref
10. Y. D. He, X. M. Zhang, J. H. You. Trans. Nonferrous Met. Soc. China. 16, 1228 (2006). Crossref
11. L. Z. Hea, X. H. Li, X. T. Liu, X. J. Wang, H. T. Zhang, J. Z. Cui. Mater. Sci. Eng. A. 527, 7510 (2010). Crossref
12. K. E. Knipling, D. C. Dunand, D. N. Seidman. Acta Mater. 56, 114 (2008). Crossref
13. V. G. Davydov, Yu. Filatov, B. Lenczowski, V. Yelagin, V. Zakharov. Non-hardenable aluminium alloy as a semi-finished product for structures. United States Patent #6,676,899. Eads Deutschland GmbH. 2004.01.13.
14. ISO Standard 13067:2011. Microbeam analysis — Electron backscatter diffraction — Measurement of average grain size.
15. P. B. Hirsch, A. Howie, R. B. Nicholson, D. W. Pashley, M. J. Whelan. Electron Microscopy of Thin Crystals. London, Butter Worths (1965) 549 p.
16. A. Cáceres, M. Casales, L. Martínez. Ingeniare. Revista chilena de ingeniería. 27 (4), 625 (2019). Crossref
17. C. Watanabe, D. Watanabe, R. Monzen. Mater. Trans. 47 (9), 2285 (2006). Crossref
18. G. Du, J. Deng, D. Yan, M. Zhao, L. Rong. J. Mater. Sci. Technol. 25 (6), 749 (2009).
19. T. Kobayashi. Mater. Sci. Eng. A. 280 (1), 8 (2000). Crossref
20. E. Avtokratova, O. Sitdikov, O. Mukhametdinova, M. Markushev, S. V. S. N. Murty, M. J. N. V. Prasad, B. P. Kashyap. J. Alloys Compd. 673, 182 (2016). Crossref
21. A. G. Mochugovskiy, A. V. Mikhaylovskaya, N. Yu. Tabachkova, V. K. Portnoy. Mater. Sci. Eng. A. 744, 195 (2019). Crossref
22. R. Angal. Corrosion and corrosion protection. Dolgoprudny, Intellect (2014) 343 p. (in Russian)